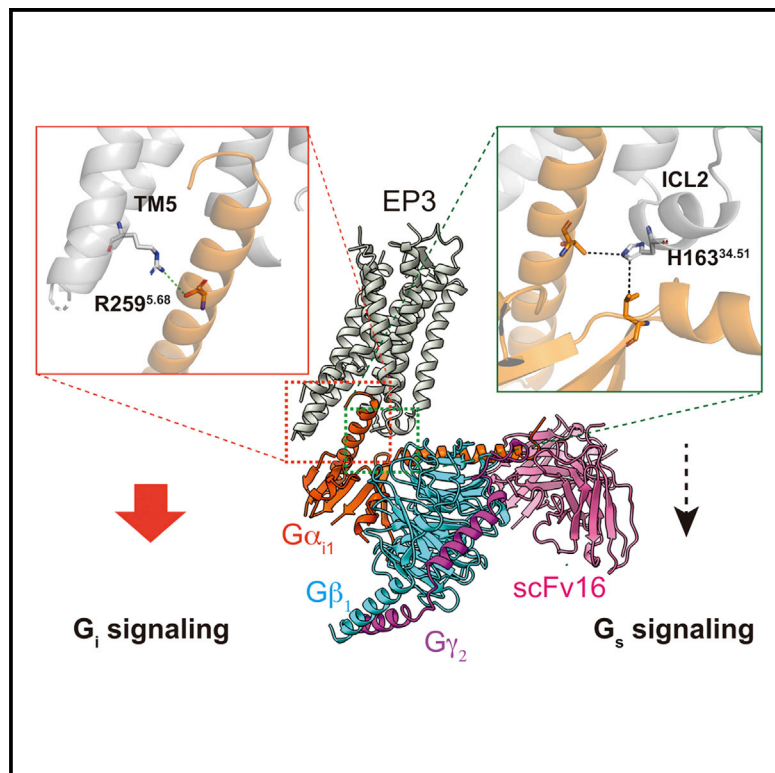


Structural insights into the G protein selectivity revealed by the human EP3-G_i signaling complex

Graphical abstract



Authors

Ryoji Suno, Yukihiro Sugita, Kazushi Morimoto, ..., Takayuki Kato, So Iwata, Takuya Kobayashi

Correspondence

sunory@hirakata.kmu.ac.jp (R.S.), kobayatk@hirakata.kmu.ac.jp (T.K.)

In brief

Suno et al. determine the structure of the prostaglandin receptor EP3-G_i signaling complex and compare it with structures of other subtype (EP2, EP4)-G_s signaling complexes. Comparing these structures, they identify amino acid residues essential for the selectivity between G_i and G_s by pharmacological analysis.

Highlights

- Determination of the structure of the human EP3-G_i signaling complex
- Identification of residues essential for G_i signaling activity of the EP3 receptor
- Identification of residues involved in G protein selectivity of PG receptors



Report

Structural insights into the G protein selectivity revealed by the human EP3-G_i signaling complex

Ryoji Suno,^{1,12,*} Yukihiro Sugita,^{2,3,4,12} Kazushi Morimoto,^{5,12} Hiroko Takazaki,² Hirokazu Tsujimoto,⁶ Mika Hirose,² Chiyo Suno-Ikeda,¹ Norimichi Nomura,⁶ Tomoya Hino,^{7,8} Asuka Inoue,⁹ Kenji Iwasaki,¹⁰ Takayuki Kato,² So Iwata,⁶ and Takuya Kobayashi^{1,11,13,*}

¹Department of Medical Chemistry, Kansai Medical University, Hirakata 573-1010, Japan

²Institute for Protein Research, Osaka University, Suita 565-0871, Japan

³Hakubi Center for Advanced Research, Kyoto University, Kyoto 606-8501, Japan

⁴Institute for Life and Medical Sciences, Kyoto University, Kyoto 606-8507, Japan

⁵Physical Chemistry for Life Science Laboratory, Faculty of Pharmaceutical Sciences, Kyushu University, Fukuoka 812-8582, Japan

⁶Department of Cell Biology and Medical Chemistry, Graduate School of Medicine, Kyoto University, Konoe-cho, Yoshida, Sakyo-ku, Kyoto 606-8501, Japan

⁷Department of Chemistry and Biotechnology, Graduate School of Engineering, Tottori University, Tottori, Japan

⁸Center for Research on Green Sustainable Chemistry, Tottori University, Tottori, Japan

⁹Graduate School of Pharmaceutical Sciences, Tohoku University, 6-3, Aoba, Aramaki, Aoba-Ku, Sendai, Miyagi 980-8578, Japan

¹⁰Life Science Center for Survival Dynamics, Tsukuba Advanced Research Alliance (TARA), University of Tsukuba, Tsukuba, Japan

¹¹Japan Agency for Medical Research and Development (AMED), Core Research for Evolutional Science and Technology (CREST), 1-7-1 Otemachi, Chiyoda-ku, Tokyo 100-0004, Japan

¹²These authors contributed equally

¹³Lead contact

*Correspondence: sunory@hirakata.kmu.ac.jp (R.S.), kobayatk@hirakata.kmu.ac.jp (T.K.)

<https://doi.org/10.1016/j.celrep.2022.111323>

SUMMARY

Prostaglandin receptors have been implicated in a wide range of functions, including inflammation, immune response, reproduction, and cancer. Our group has previously determined the crystal structure of the active-like EP3 bound to its endogenous agonist, prostaglandin E₂. Here, we present the single-particle cryoelectron microscopy (cryo-EM) structure of the human EP3-G_i signaling complex at a resolution of 3.4 Å. The structure reveals the binding mode of G_i to EP3 and the structural changes induced in EP3 by G_i binding. In addition, we compare the structure of the EP3-G_i complex with other subtypes of prostaglandin receptors (EP2 and EP4) bound to G_s that have been previously reported and examine the differences in amino acid composition at the receptor-G protein interface. Mutational analysis reveals that the selectivity of the G protein depends on specific amino acid residues in the second intracellular loop and TM5.

INTRODUCTION

Prostaglandin E₂ (PGE₂) is an important lipid mediator that is metabolized by cyclooxygenase (COX) in inflammatory and immune responses and acts on four prostaglandin E (EP) receptor subtypes (EP1–EP4), which are G protein-coupled receptors (GPCRs) (Norel et al., 2020). Among these prostaglandin receptor subtypes, the EP3 receptor subtype is involved in smooth muscle contraction, thrombosis and angiogenesis, fever generation, etc. PGE₂ induces increased vascular permeability and neutrophil mobilization via EP3 receptors on mast cells, resulting in swelling (Morimoto et al., 2014). These vital functions of EP3 makes it an important drug target, and therefore understanding its signaling through G protein can provide useful information for treating several diseases, including angle glaucoma and ocular hypertension (Suto et al., 2015).

The most important signaling pathways of the EP3 receptor include the inhibition of adenylate cyclase by G_i and G_i-depen-

dent phospholipase C (PLC) activation. On the other hand, the EP2 and EP4 receptors are G_s coupled and cause an increase in cAMP concentration. The EP receptor subtype EP1 receptor induces intracellular Ca²⁺ mobilization via G_q proteins (Norel et al., 2020).

Recent advances in the cryoelectron microscopy (cryo-EM) technique have enabled high-resolution structure determination of various GPCR-signal transducer complexes. These structures have revealed details of the activation mechanism of GPCRs by G proteins as well as the binding modes of their ligands (García-Nafria and Tate, 2020). While each GPCR binds selectively to a specific subtype of Gα subunit, how this selectivity is regulated is not fully understood. It has been reported that the length of transmembrane 5 (TM5) and TM6 is important for the selectivity of G_s and G_i at serotonin receptors (Huang et al., 2022). Biochemical analyses of cannabinoid and prostaglandin receptors have shown that specific amino acid residues in the intracellular loop 2 (ICL2) contribute to their G protein selectivity



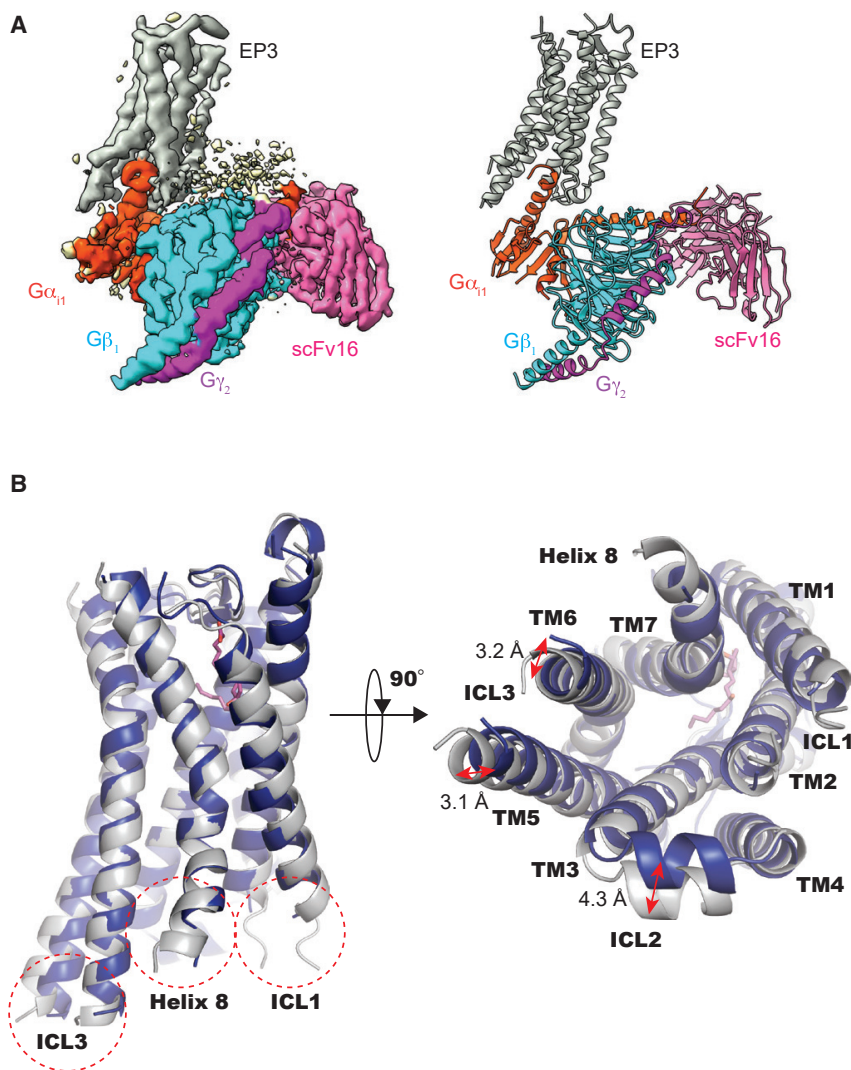


Figure 1. Cryo-EM structure of the human EP3-G_i-scFv16 complex

(A) Side view of the cryo-EM density map (left) and model (right) of the human EP3-G_i-scFv16 complex (gray, EP3; orange, G_i; cyan, G_β; purple, G_γ; pink, scFv16). Density maps in yellow are considered random noise.

(B) Side (left) and intracellular (right) views of active-like EP3 (blue, PDB: 6AK3; PGE₂, magenta) and the G_α₁₁-bound active state of EP3 (gray). The region surrounded by the red dotted line is the newly determined region in the EP3-G_i complex structure.

or G_s also interact with G proteins at amino acid positions 34.51 and 5.68 (Xiao et al., 2021; Xu et al., 2021; Yin et al., 2020; Zhuang et al., 2021). Overall, these results suggest that the amino acid residues at positions 34.51 and 5.68 may play an important role in the G protein selectivity among class A GPCR family.

RESULTS AND DISCUSSION

Cryo-EM structure of human EP3-G_i signaling complex

In order to obtain a stable human EP3-G_i signaling complex, PGE₂-bound human EP3-GFP was incubated with heterotrimeric G_i. The complex was treated with apyrase, and the human EP3-GFP-PGE₂-G_i complex was purified using anti-GFP nanobody affinity chromatography. A single-stranded variable fragment (scFv16) was added to bind to the G_α_i-G_β interface and stabilize the complex of nucleotide-free G_i and EP3 (Maeda et al., 2018). The human EP3-PGE₂-G_i-scFv16 complex

was then purified to homogeneity by gel filtration chromatography (Figure S1).

The structure of the human EP3-G_i signaling complex was determined at a resolution of 3.4 Å from 125,572 particles (Figure S2). This allowed us to accurately identify and assign the TM domain (TMD) of EP3, the G_i protein, and the antibody fragment in the cryo-EM map (Figures 1A and S3A). The refined structure of the human EP3-G_i signaling complex contained residues 49–357 of EP3, 4–40, 182–201, 207–225, 249–269, and 317–354 of G_i, 5–340 of G_β, and 9–61 of G_γ. The local resolution map shows that the resolution of the receptor domain is relatively low compared with the overall structure of the EP3-G_i complex, suggesting conformational heterogeneity (Figure S3B). In particular, the extracellular and the ligand binding region of EP3 displayed weak cryo-EM densities. The amino acid residues 81–82 of ICL1, 118–119 of extra cellular loop 1 (ECL1), 266–269 of ICL3, and 309–322 of ECL3 could not be modeled because of their inherent flexibility (Figure S4). Similarly, the cryo-EM density of the alpha-helical domain (AHD) of G_i was barely visible

(Chen et al., 2010; Sugimoto et al., 2004). However, there are few reports of structural analysis of GPCR-G protein complexes, in which G protein selectivity was discussed with a focus on specific amino acids.

Structural studies of EP2-G_s and EP4-G_s complexes have provided insights into the binding modes of each receptor to its ligand and their mechanisms of activation by G_s (Nojima et al., 2021; Qu et al., 2021). In order to expand our knowledge of prostaglandin receptor complexes, we report the cryo-EM structure of the human EP3-G_i signaling complex (human EP3-G_α_iβ₁γ₂) at 3.4 Å resolution. Mutational analysis of prostaglandin receptors using cAMP activity assays revealed the identity of amino acid residues in EP3 that are important for its selectivity between G_i and G_s binding. Those amino acids are the residues located at position 34.51 of ICL2 in EP3 and at position 5.68 of TM5 in EP4 (as per Ballesteros-Weinstein numbering). Substitution of each of these amino acids with the corresponding residues in EP4/EP3 suppressed the signaling of the G protein subtype to which they are coupled. Similarly, dopamine receptors that couple to G_i

because of its intrinsically flexible nature in the absence of GDP/GTP. The cryo-EM density of PGE₂ was also barely visible.

Overall structure of human EP3-G_i signaling complex

The final density map of the human EP3-G_i signaling complex revealed several previously unseen regions including residues 78–80 and 83–85 of ICL1, 265 and 270 of ICL3, 308 of ECL3, and 356–357 of helix 8, which were not resolved in the structure of PGE₂-bound EP3 alone. The overall structure of the G_i-bound EP3 is similar to the active-like form of EP3 (PDB: 6AK3) bound to PGE₂ (root-mean-square deviation of 1.061 Å) (Figure 1B, left). A detailed comparison of the G_i-bound/unbound states of EP3 revealed some structural changes at the EP3-G_i interface. First, the ICL2 of G_i-bound EP3 was shifted outwards by 4.3 Å compared with the active-like EP3. Second, TM5 and TM6 were extended outwards in the G_i-bound structure (3.1 and 3.2 Å, respectively) (Figure 1B, right). In both cases, EP3 was bound to PGE₂, suggesting that the additional conformational changes in G_i-bound EP3 are induced exclusively by G_i binding.

The EP3-G_i interface

The human EP3-G_i signaling complex is formed primarily by two interfaces between EP3 and G_i. The first interface is formed by a portion of the C-terminal α5 helix of G_i (T340–F354), which enters the central cytoplasmic cavity of EP3 through the gap between TM2, TM3, TM5, and TM6 (Figures 2A, 2B, and S5A). The second interface is comprised of the ICL2 of EP3, which interacts with the N-terminal helix and the C-terminal α5 helix of the G_i (Figures 2C and S5A). The C-terminal α5 helix shows hydrophobic or van der Waals interactions with TM2, TM3, TM6, and ICL2 residues (TM2: F88^{2.39}, TM3: A158^{3.53}, I159^{3.54}, ICL2: P162^{34.50}, Y165^{34.53}, TM6: W273^{6.26}, T280^{6.33}; Ballesteros-Weinstein numbering is shown in superscript) (Figure S5A). Although the EM density around the side chain of E279^{6.32} is weak, the side chain of E279^{6.32} is close enough to interact with the carbonyl group of L353 (Figure 2A). The side chains of R259^{5.68} and Q283^{6.36} form hydrogen bonds with the side chain of T340 and the carbonyl group of L353 of G_i, respectively (Figures 2A, 2B, and S5A). The GPCR family contains several conserved motifs important for receptor activation, such as the DRY motif (E^{3.49}R^{3.50}A^{3.51} in EP3) and the NPXXY motif (D^{7.49}P^{7.50}XY^{7.53}) (Weis and Kobilka, 2018). The amino acid residues E154^{3.49} and R155^{3.50} are part of the DRY motif and form hydrogen bonds with the side chain and carbonyl group of C351 of G_i, respectively. Y165^{34.53} forms van der Waals interactions and hydrogen bonds with the side chains of N347 and C351 of G_i, respectively (Figures 2A and S5A). Interestingly, H163^{34.51} forms van der Waals interactions with the side chain of L194, which is located in the β sheet 3 of G_i (Figures 2C and S5A).

The role of these amino acids in human EP3-G_i signaling was examined by mutagenesis and cAMP signaling assays (Figure 2D; Table S1). Among the tested mutants, F88^{2.39}M, R155^{3.50}A, E279^{6.32}A, and Q283^{6.36}A displayed significantly reduced cAMP signaling activity. F54^{2.39} of EP4, analogous to F88^{2.39} of EP3, has been reported to be important for the G_s-mediated signaling (Nojima et al., 2021). As expected, F88^{2.39}M of EP3 was found to affect G_i-mediated signaling. Although F88^{2.39} is close to the main chain of C351 and G352 of G_i, the EM density for the side

chain of F88^{2.39} is weak, and therefore it is unclear how it interacts with G_i (Figure S6). As observed with other GPCRs (Weis and Kobilka, 2018), the mutation of R155^{3.50} in the DRY motif, an essential amino acid for signal transduction, affected the G_i signaling. The reduced signal activity of mutant E279^{6.32}A suggested the role of E279^{6.32} in G_i signaling. Overall, these results, taken together with the cryo-EM structure of the EP3-G_i complex, show the importance of polar interactions between EP3 and the C-terminal residues of G_i (C351–L353) (so-called "wavy hook") (Kim et al., 2020a) for downstream signaling activity (Figures 2A, 2D, and S5A; Table S1).

Next, we examined residues Y165^{34.53} (ICL2), R259^{5.68} (TM5), and W273^{6.26} (TM6) of EP3 that interact exclusively with the helical region of α5 helix and not the wavy-hook region. Alanine mutants were produced for these amino acids. Additionally, the R^{5.68}M mutant was generated since EP4 contains a methionine at position 5.68. The R259^{5.68}A, R259^{5.68}M, and W273^{6.26}A mutants slightly reduced G_i-mediated signaling activity (pEC₅₀ = 9.32 ± 0.14, 9.51 ± 0.04, and 9.13 ± 0.11, respectively) relative to the wild type (pEC₅₀ = 9.87 ± 0.08). The side chains of R259^{5.68} and W273^{6.26} interact with one another as shown in Figure 2B. The double mutants R259^{5.68}A/W273^{6.26}A and R259^{5.68}M/W273^{6.26}A had lower signaling activity (pEC₅₀ = 8.50 ± 0.10 and 8.72 ± 0.10, respectively) than the single mutants (Figures 2E and S5A). The double mutants Y165^{34.53}A/R259^{5.68}A, Y165^{34.53}A/R259^{5.68}M, and Y165^{34.53}A/W273^{6.26}A showed further reduction in signaling activity (pEC₅₀ = 8.48 ± 0.12, 9.14 ± 0.06, and 8.65 ± 0.08, respectively). Notably, the triple mutant Y165^{34.53}A/R259^{5.68}A/W273^{6.26}A showed the highest reduction in signaling activity with a pEC₅₀ of 6.71 ± 0.98 (Figures 2F and S5A). The triple mutant Y165^{34.53}A/R259^{5.68}M/W273^{6.26}A also showed slightly less signaling activity (pEC₅₀ = 8.40 ± 0.18) than the double mutant (Figures 2F and S5A). These results suggest that Y165^{34.53}, R259^{5.68}, and W273^{6.26} cooperatively contribute to G_i binding, stabilization of the EP3-G_i complex, and downstream signaling (Table S1). On the other hand, electrostatic interactions have been shown to be one of the key driving forces for coupling between GPCRs and G_i proteins (Xu et al., 2021). Surface charge properties at the EP2/EP4-G_s and EP3-G_i interfaces are shown in Figure S7. Comparison between these GPCR-G protein interfaces shows that EP3, which couples with G_i, has a large region of positive charge, while the surface charge of EP2, which couples only with G_s, has a smaller region of positive charge. EP4, which binds to both G_i and G_s, was found to have a region of positive charge that is narrower than EP3 but significantly larger than EP2. This suggests that G_i preferably binds to GPCRs with a larger area of positive charge, such as EP3, through electrostatic interactions (Figure S7).

Furthermore, we investigated if amino acid residues at positions 5.68 (Ballesteros-Weinstein numbering) in other GPCRs affect their G protein signaling. The analysis was performed on μ-opioid receptor (MOR), dopamine receptor D2 (D2R), D3R, cannabinoid receptor type 1 (CB1), CB2, and α2B receptors in complex with G_i protein (Hua et al., 2020; Koehl et al., 2018; Vecchio et al., 2018; Xing et al., 2020; Xu et al., 2021; Yuan et al., 2020; Zhuang et al., 2021). Dopamine and cannabinoid receptors were compared because they are coupled with G_i and G_s like prostaglandin receptors (EP2, EP3, and

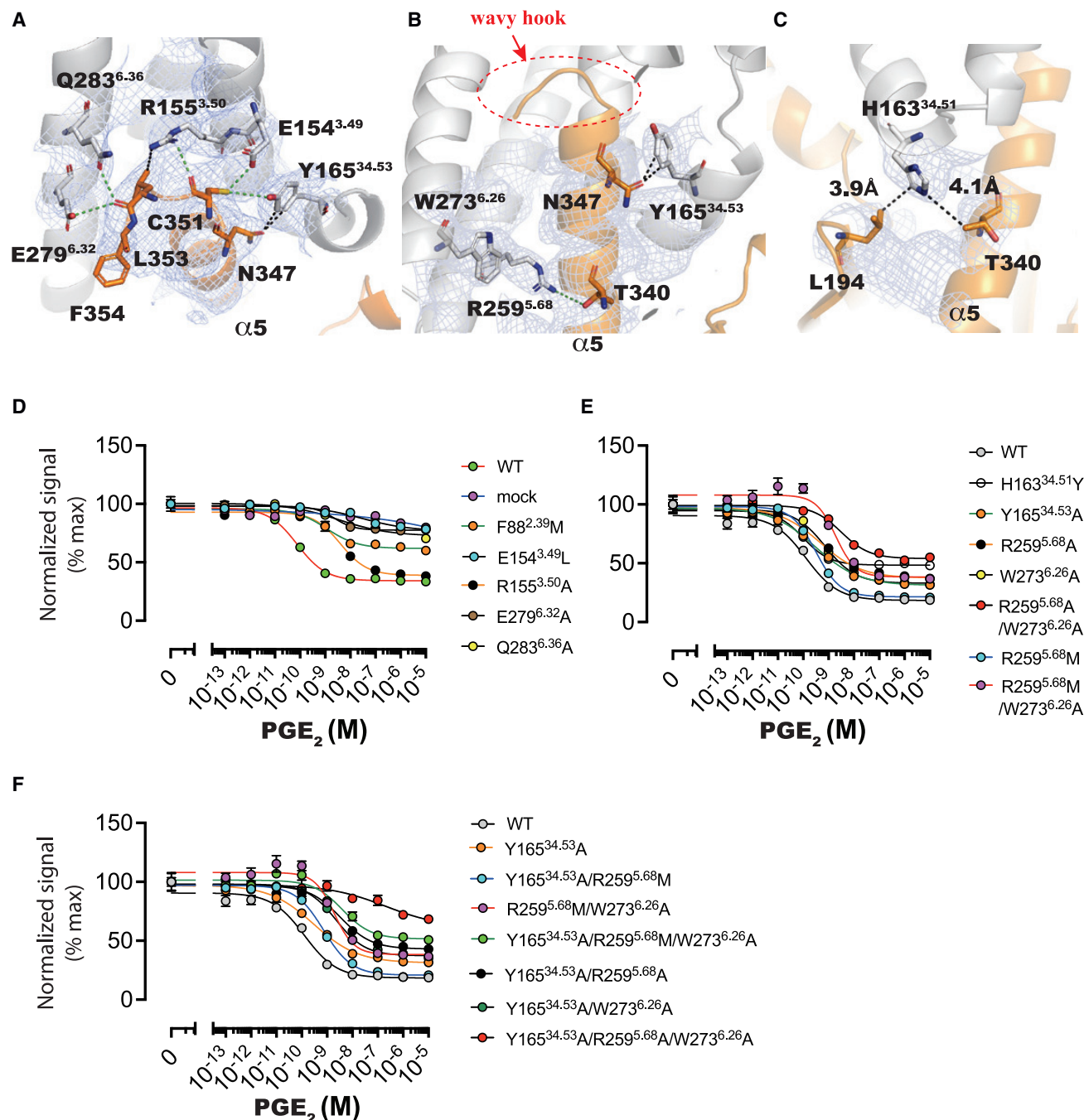


Figure 2. Interactions between EP3 and G_i

(A–C) Interactions between G_i (orange) and TM3, TM5, TM6, and ICL2 of EP3 receptor (gray). The cryo-EM density for the displayed amino acids is represented as a blue mesh with a contour of 4σ.

(D–F) Effects of mutations in EP3 on its G_i-mediated signaling. Nonpolar and polar interactions are displayed as black and green dotted lines, respectively. Each data point is represented as the mean, with the error bars showing ± SEM (n = 3 separate signaling assays).

EP4) depending on their subtypes (Figure S5B). A comparison of these GPCRs with the EP3 receptor showed the conserved nature of the DRY motif and its interaction with the Gα subunit, but no other similarities common to all these GPCRs were apparent. However, a local comparison between these

GPCRs did reveal a few commonalities. Particularly for dopamine receptors, we found that both D2R and D3R bind G_i at the same amino acids as EP3. As observed in EP3, R219^{5.68} in D2R and R218^{5.68} in D3R interact with T340 of G_i (Figures S5B and S8A–S8C).

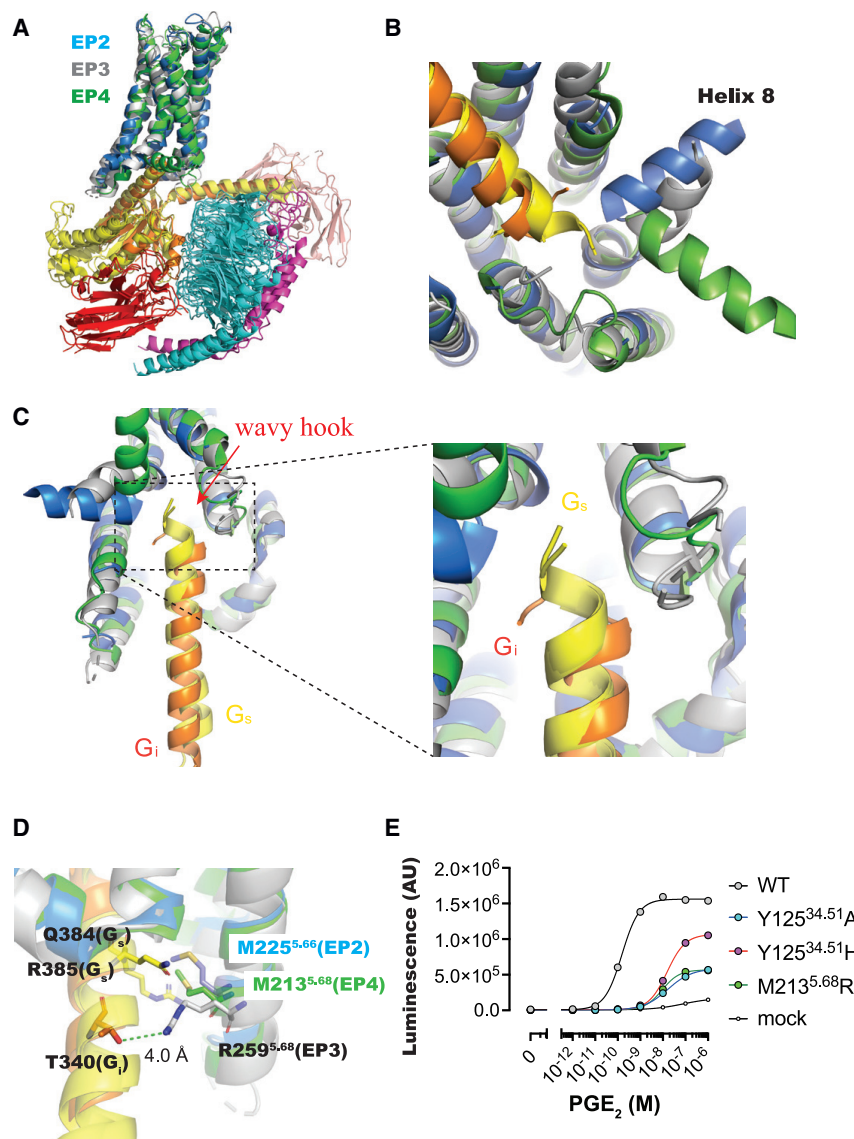


Figure 3. G protein selectivity of prostaglandin receptors by amino acid at position 5.68

(A) Side view of EP2 (blue, PDB: 7CX2), EP3 (gray), and EP4 (green, PDB: 7D7M); orange, G_i bound to EP3; yellow, G_s bound to EP2 or EP4; cyan, G₁₂; purple, G₁₂; pink, scFv16; red, Nb35. (B) Orientation of helix 8 of each EP receptor and position of the C-terminal $\alpha 5$ helix of G proteins. (C) Differences in binding modes between G_i and G_s $\alpha 5$ helix to prostaglandin receptors. (D) Differences in the binding mode of the amino acid at position 5.68 of EP3 and the corresponding amino acid of EP2 and EP4 to the G protein. (E) Effect of mutations at positions 5.68 and 34.51 on G_s-mediated signaling of EP4. Each data point is represented as the mean, with the error bars showing \pm SEM (n = 3 separate signaling assays).

penetrating further into the receptor than that of G_i (Figure 3C). More amino acid residues were observed in the $\alpha 5$ helix of G_s interacting with EP2 and EP4 than in the $\alpha 5$ helix of G_i interacting with EP3 (Figure S5A). Thus, the EP receptors have different binding modes to G_i and G_s.

The structural comparison between EP receptor-G protein complexes shows that TM5^{5.66} in EP2 is analogous to TM5^{5.68} in both EP3 and EP4 (Figures 3D and S9). Among the amino acid residues of the EP receptors that interact with the G protein, TM5^{5.68} and ICL2^{34.51} are common in EP2 and EP4 but different in EP3. Several amino acid residues in the TM5 of both EP2 and EP4 interact with G_s. In contrast, only R259^{5.68} in the TM5 of EP3 interacts with G_i (Figure S5A). A swap mutant of EP4, M213^{5.68}R was generated by replacing M213^{5.68} of EP4 with an arginine residue as found in the EP3 receptor. The M213^{5.68}R mutant of EP4 markedly reduced the G_s-

Role of TM5^{5.68} in G protein selectivity of prostaglandin receptors

To understand the difference between the activation mechanisms of the EP receptor family, we superimposed the structures of PGE₂-bound EP2-G_s, EP3-G_i, and EP4-G_s (Figure 3A). EP1 could not be compared because its high-resolution structure has not yet been determined. The structural comparison showed that the orientation of helix 8 is different in each EP receptor-G protein complex. The C terminus of the wavy hook of G_s is close to the helix 8 of EP2/EP4, and they interact, whereas the helix 8 of EP3 is oriented away from the C terminus of the wavy hook of G_i, and they do not interact (Figure 3B). Although the C-terminal (R381-L393) orientation of G_s $\alpha 5$ helix was the same for both EP2 and EP4, the orientation of the $\alpha 5$ helix of G_i for EP3 was significantly different. The position and orientation of the C-terminal wavy hook, which is important for G protein signaling activity, also differed between EP2/EP4-bound G_s and EP3-bound G_i, with the wavy hook of G_s

mediated signaling activity (pEC₅₀ = 8.98 \pm 0.02) compared with the wild type (pEC₅₀ = 10.48 \pm 0.02), suggesting that the amino acid at position 5.68 is involved in selectivity between G_s and G_i (Figure 3E; Table S2). M213^{5.68} of EP4 interacts with Q384 and R385 of G_s $\alpha 5$ helix (Figure S9C), and it is possible that the side chain of the arginine residue in M213^{5.68}R EP4 mutant cause steric hindrance with R385 of G_s. This would suggest that EP3 is more likely to bind to G_i than G_s. As mentioned above, superimposed structures of EP2-G_s and EP3-G_i show that R259^{5.68} of EP3 is in the same position as M225^{5.66} of EP2. Moreover, the amino acid position at 5.66 is occupied by a methionine residue in other prostaglandin receptors such as DP1 and IP subtypes that primarily bind to G_s. This further suggests that prostaglandin receptors that bind to G_s have a conserved methionine at position 5.66. As an example of another GPCR, the amino acid residue at position 5.68 in NTSR1, which is coupled with both G_{i/o} and G_s, is methionine, as is EP4 (Kato et al., 2019).

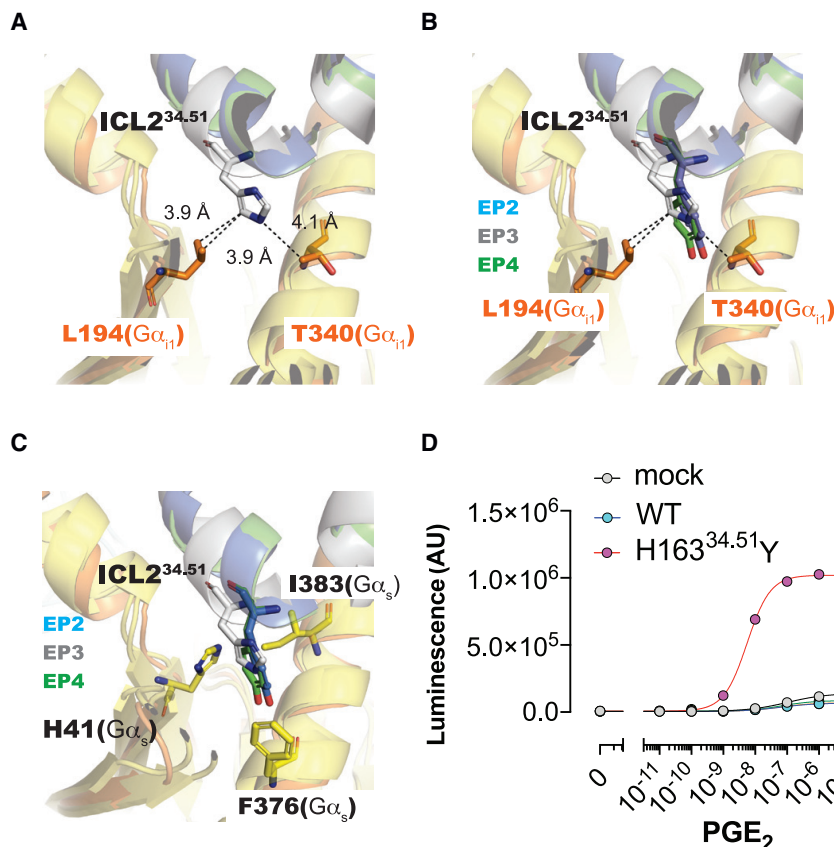


Figure 4. G protein selectivity of prostaglandin receptors by amino acid at position 34.51 of ICL2

(A–C) The interactions between prostaglandin receptors and G α subunits; EP2 (blue, PDB: 7CX2); EP3 (gray); EP4 (green, PDB: 7D7M); orange, G α bound to EP3; yellow, G α bound to EP2 or EP4. (D) Effect of mutation at position 34.51 on G α -mediated signaling of EP3. Each data point is represented as the mean, with the error bars showing \pm SEM (n = 3 separate signaling assays).

Similar to the prostaglandin receptor subtypes (EP2, EP3, and EP4), dopamine receptors show either G $\alpha_{i/o}$ or G α_s selectivity depending on the subtype. Several structures of dopamine receptors bound to G proteins have been recently determined, including D1R-G α_s , D2R-G α_i , and D3R-G α_i (Yin et al., 2020; Zhuang et al., 2021). The structural superimposition of these complexes shows that Q224^{5.68} in D1R interacts with Q384 and R385 of G α_s (Figures S8A and S8D). Notably, both D2R and D3R, which couple with G α_i , have an arginine residue at amino acid position 5.68, as observed in EP3 (Figures S8A–S8C and S9A). This striking similarity between dopamine receptors and prostaglandin receptors clearly suggests that the amino acid at position 5.68 plays a role in regulating G protein selectivity.

Role of ICL2^{34.51} in G protein selectivity of prostaglandin receptors

It has been reported that Y^{34.51} of mouse EP2 is crucial for G α_s binding and plays an important role in the mechanism of G protein selectivity among prostaglandin receptors. Furthermore, it has been reported that the substitution of H^{34.51} with tyrosine in mouse EP3 receptor results in G α_s -mediated activity (Sugimoto et al., 2004). In this study, we found that the H163^{34.51}Y mutant of human EP3 also showed an increased G α_s -mediated activity and a slight inhibition of G α_i -mediated activity (Figures 2E and 4D). We also observed reduced G α_s -mediated activities of the Y125^{34.51}A and Y125^{34.51}H mutants of human EP4, confirming that this residue is important for G α_s -mediated signaling activity (Figure 3E). In

the cryo-EM structure of the human EP3-G α_i signaling complex, H163^{34.51} interacts with the side chain of L194 in the β 2- β 3 loop and T340 in the α 5 helix of G α_i (Figures 4A and 4B). In the superimposed view of the structures of the EP2-G α_s and EP4-G α_s with EP3-G α_i , the distance between the side chain of H163^{34.51} in EP3 and G α_s is far apart (Figure 4C). The side chain of the tyrosine residue in the H163^{34.51}Y mutant of EP3 was suggested to interact with the hydrophobic pocket of G α_s , similar to the side chain of Y^{34.51} in both EP2 and EP4 (Figure 4C). When prostaglandin receptors are classified based on their coupling with G α subtypes, G α_s -bound prostaglandin receptors have either tyrosine or phenylalanine at position 34.51 (Figure S5C). On the other

hand, EP3 is the prostaglandin receptor that couples with G $\alpha_{i/o}$ and G $\alpha_{12/13}$. A unique feature of EP3 is that the amino acid at position 34.51 is a histidine, unlike other prostaglandin receptors. In order to couple with both G $\alpha_{i/o}$ and G $\alpha_{12/13}$, the amino acid at position 34.51 may need to be histidine. GPCRs that feature a histidine residue at position 34.51 of ICL2 are OXE, HCA1-3, GPR82, and GPR152. Among them, OXE and HCA1-3 are reported to bind mainly G $\alpha_{i/o}$ family G proteins (Hosoi et al., 2002; Liu et al., 2009; Wise et al., 2003), suggesting that a histidine located at position 34.51 could be linked to G $\alpha_{i/o}$ coupling. As another example of a GPCR, the cannabinoid receptor, which is primarily a G α_i -coupled receptor, markedly increases its G α_s -mediated signaling activity by an amino acid mutation at position 34.51 (Chen et al., 2010). Dopamine receptors, like prostaglandin receptors (EP2, EP3, and EP4), bind to one of two G α subunit subtypes (G α_i or G α_s) depending on the receptor subtype. In the case of the D1R-G α_s complex, the side chain at F129^{34.51} of D1R enters deep into the pocket of G α_s , analogous to Y125^{34.51} and Y142^{34.51} in the structure of EP2-G α_s and EP4-G α_s , respectively (Figures S5B, S5C, and S8E). On the other hand, in D2R and D3R, which bind mainly G α_i but not to G α_s , the amino acids at position 34.51 are methionine and valine residues, respectively (Xu et al., 2021), and do not form strong interactions with G proteins as in EP3 (Figure S8F). Thus, in dopamine receptors, as in prostaglandin receptors, the amino acid at position 34.51 may contribute to the selectivity between G α_s and G $\alpha_{i/o}$. In HTR2A, ICL2 has been reported to be involved in signal

selectivity between G proteins and arrestin, suggesting that ICL2 may contribute to the selectivity between different effector molecules (Kim et al., 2020b).

DISCUSSION

The comparison of the newly determined EP3-G_i complex with EP2-G_s and EP4-G_s complexes along with the mutational analysis revealed important amino acids involved in the G protein selectivity of prostaglandin receptors. There are several reports that describe the importance of ICL2 for G protein binding and selectivity. In G_s-coupled GPCRs, the side chains of phenylalanine or tyrosine residue at position 34.51 of ICL2 strongly interact with the side chains of several amino acids of G_s (Kim et al., 2020a). This is also true for prostaglandin receptors, and structural biology revealed that the side chain of amino acid at position 34.51 determines the selectivity of G α subunits. Furthermore, in prostaglandin receptors, the arginine residue at position 5.68 was found to affect the selectivity and binding to G_i and G_s, suggesting that other GPCRs such as dopamine receptors may have similar properties. The striking similarity found in the molecular determinants of G protein selectivity between prostaglandin and dopamine receptors points to a broader applicability to class A GPCRs. There is also interest in the selectivity of G proteins at various receptors other than GPCRs coupled to G_i and G_s. For example, a combination of structural information and pharmacological analysis revealed that the lipid-CKK1R interaction affects the selectivity between G_s and G_i binding (Mobbs et al., 2021). To elucidate the mechanism of selective signaling, it is necessary to determine and compare the complex structures of various signaling factors with the same receptor. The structural information will not only reveal the molecular mechanism of each signal transduction but also provide important insights for the development of drugs such as biased ligands.

Limitations of the study

In the present study, a structural comparison of three prostaglandin receptor-G protein complexes and supporting pharmacological experiments revealed the amino acid residues that affect G_s versus G_i selectivity. However, the measurement of signaling activity of mutants for G_s and G_i protein was performed only on the prostaglandin receptors, and further validation is needed to determine whether similar amino acid residues are involved in the G protein selectivity in other GPCRs, including dopamine receptors.

STAR★METHODS

Detailed methods are provided in the online version of this paper and include the following:

- KEY RESOURCES TABLE
- RESOURCE AVAILABILITY
 - Lead contact
 - Materials availability
 - Data and code availability
- EXPERIMENTAL MODEL AND SUBJECT DETAILS
- METHOD DETAILS

- Expression and purification
- Formation and purification of the human EP3-G_iG β γ ₂-scFv16 complex
- Cryo-EM grid preparation and data collection
- Image processing
- Model building and refinement
- Signaling assay

● QUANTIFICATION AND STATISTICAL ANALYSIS

SUPPLEMENTAL INFORMATION

Supplemental information can be found online at <https://doi.org/10.1016/j.celrep.2022.111323>.

ACKNOWLEDGMENTS

The plasmids for expressing G_i and G β γ ₂ were provided by Brian K. Kobilka (Stanford University). This research was supported by Platform Project for Supporting Drug Discovery and Life Science Research (Basis for Supporting Innovative Drug Discovery and Life Science Research [BINDS]) from AMED (JP21am0101072 [support number 1113] to K.I. and T. Kato, and JP19am0101079 [support number 2365] to S.I.); the Takeda Science Foundation (to R.S., Yuijnk.S., K.M., and T. Kobayashi); Ono Medical Research Foundation (to K.M.); AMED Core Research for Evolutional Science and Technology (CREST) (JP21gm0910007 to T. Kobayashi); AMED Science and Technology Platform Program for Advanced Biological Medicine under grant number JP21am0401020 (to T. Kobayashi); AMED Research on Development of New Drugs (JP20ak0101103 to T. Kobayashi); The Naito Foundation (to T. Kobayashi); Koyanagi Foundation (to T. Kobayashi); FOREST Program JPMJFR215T (to A.I.); JST Moonshot Research and Development Program JPMJMS2023 (to A.I.) from Japan Science and Technology Agency (JST), JSPS KAKENHI (15K08268 and 19H03428 to R.S.; 20H03434 to K.M.; and 21H04791, 21H05113, and JPJSBP120218801 to A.I.); and a Grant-in-Aid for Transformative Research Areas (21H05112 to R.S.) and for MEXT LEADER Program (to Y.S.). DNA sequencing analysis was performed at the Medical Research Support Center, Graduate School of Medicine at Kyoto University.

AUTHOR CONTRIBUTIONS

R.S., H.T., and C.S.-I. carried out protein expression and purification of the receptors, G proteins, and GFP nanobody. N.N. purified scFv16 fragment. T.H. provided the plasmids for expressing GFP nanobody and purified GFP nanobody. R.S. prepared the cryo-EM sample of EP3-G_i-scFv16 complex. K.M. and A.I. carried out the signaling assays. R.S., Y.S., and M.H. carried out the cryo-EM data collection. Y.S. and H.T. carried out cryo-EM data processing and model building of EP3-G_i-scFv16 complex. R.S. designed the project, and K.I., T. Kato., T. Kobayashi, and S.I. supervised the overall project. R.S., Y.S., and K.M. wrote the manuscript. All authors discussed the results and commented on the manuscript.

DECLARATION OF INTERESTS

The authors declare no competing financial interests.

Received: March 28, 2022

Revised: July 18, 2022

Accepted: August 17, 2022

Published: September 13, 2022

REFERENCES

Adams, P.D., Afonine, P.V., Bunkóczi, G., Chen, V.B., Davis, I.W., Echols, N., Headd, J.J., Hung, L.W., Kapral, G.J., Grosse-Kunstleve, R.W., et al. (2010). PHENIX: a comprehensive Python-based system for macromolecular structure solution. *Acta Crystallogr. D Biol. Crystallogr.* 66, 213–221.

- Chen, X., Yang, W., Fan, Y., Luo, J.S., Hong, K., Wang, Z., Yan, J.F., Chen, X., Lu, J.X., Benovic, J.L., and Zhou, N.M. (2010). Structural determinants in the second intracellular loop of the human cannabinoid CB1 receptor mediate selective coupling to Gs and Gi. *Br. J. Pharmacol.* **161**, 1817–1834.
- Emsley, P., Lohkamp, B., Scott, W.G., and Cowtan, K. (2010). Features and development of Coot. *Acta Crystallogr. D Biol. Crystallogr.* **66**, 486–501.
- García-Nafria, J., and Tate, C.G. (2020). Cryo-electron microscopy: moving beyond X-ray crystal structures for drug receptors and drug development. *Annu. Rev. Pharmacol. Toxicol.* **60**, 51–71.
- Hosoi, T., Koguchi, Y., Sugikawa, E., Chikada, A., Ogawa, K., Tsuda, N., Suto, N., Tsunoda, S., Taniguchi, T., and Ohnuki, T. (2002). Identification of a novel human eicosanoid receptor coupled to Gi/o. *J. Biol. Chem.* **277**, 31459–31465.
- Hua, T., Li, X., Wu, L., Iliopoulos-Tsoutsouvas, C., Wang, Y., Wu, M., Shen, L., Brust, C.A., Nikas, S.P., Song, F., et al. (2020). Activation and signaling mechanism revealed by cannabinoid receptor-gi complex structures. *Cell* **180**, 655–665.e18.
- Huang, S., Xu, P., Shen, D.-D., Simon, I.A., Mao, C., Tan, Y., Zhang, H., Harpsøe, K., Li, H., Zhang, Y., et al. (2022). GPCRs steer Gi and Gs selectivity via TM5-TM6 switches as revealed by structures of serotonin receptors. *Mol. Cell* **82**, 2681–2695.e6.
- Kato, H.E., Zhang, Y., Hu, H., Suomivuori, C.M., Kadji, F.M.N., Aoki, J., Krishna Kumar, K., Fonseca, R., Hilger, D., Huang, W., et al. (2019). Conformational transitions of a neurotensin receptor 1-Gi1 complex. *Nature* **572**, 80–85.
- Kim, H.R., Xu, J., Maeda, S., Duc, N.M., Ahn, D., Du, Y., and Chung, K.Y. (2020a). Structural mechanism underlying primary and secondary coupling between GPCRs and the Gi/o family. *Nat. Commun.* **11**, 3160.
- Kim, K., Che, T., Panova, O., DiBerto, J.F., Lyu, J., Krumm, B.E., Wacker, D., Robertson, M.J., Seven, A.B., Nichols, D.E., et al. (2020b). Structure of a hallucinogen-activated Gq-coupled 5-HT2A serotonin receptor. *Cell* **182**, 1574–1588.e19.
- Koehl, A., Hu, H., Maeda, S., Zhang, Y., Qu, Q., Paggi, J.M., Latorraca, N.R., Hilger, D., Dawson, R., Matile, H., et al. (2018). Structure of the μ -opioid receptor-Gi protein complex. *Nature* **558**, 547–552.
- Liu, C., Wu, J., Zhu, J., Kuei, C., Yu, J., Shelton, J., Sutton, S.W., Li, X., Yun, S.J., Mirzadegan, T., et al. (2009). Lactate inhibits lipolysis in fat cells through activation of an. *J. Biol. Chem.* **284**, 2811–2822.
- Maeda, S., Koehl, A., Matile, H., Hu, H., Hilger, D., Schertler, G.F.X., Manglik, A., Skiniotis, G., Dawson, R.J.P., and Kobilka, B.K. (2018). Development of an antibody fragment that stabilizes GPCR/G-protein complexes. *Nat. Commun.* **9**, 3712–3719.
- Mobbs, J.I., Belousoff, M.J., Harikumar, K.G., Piper, S.J., Xu, X., Furness, S.G.B., Venugopal, H., Christopoulos, A., Danev, R., Wootten, D., et al. (2021). Structures of the human cholecystokinin 1 (CCK1) receptor bound to Gs and Gq mimetic proteins provide insight into mechanisms of G protein selectivity. *PLoS Biol.* **19**, e3001295–28.
- Morimoto, K., Shirata, N., Taketomi, Y., Tsuchiya, S., Segi-Nishida, E., Inazumi, T., Kabashima, K., Tanaka, S., Murakami, M., Narumiya, S., and Sugimoto, Y. (2014). Prostaglandin E2 –EP3 signaling induces inflammatory swelling by mast cell activation. *J. Immunol.* **192**, 1130–1137.
- Morimoto, K., Suno, R., Hotta, Y., Yamashita, K., Hirata, K., Yamamoto, M., Narumiya, S., Iwata, S., and Kobayashi, T. (2019). Crystal structure of the endogenous agonist-bound prostanoid receptor EP3. *Nat. Chem. Biol.* **15**, 8–10.
- Nojima, S., Fujita, Y., Kimura, K.T., Nomura, N., Suno, R., Morimoto, K., Yamamoto, M., Noda, T., Iwata, S., Shigematsu, H., and Kobayashi, T. (2021). Cryo-EM structure of the prostaglandin E receptor EP4 coupled to G protein. *Structure* **29**, 252–260.e6.
- Norel, X., Sugimoto, Y., Ozen, G., Abdelazeem, H., Amgoud, Y., Bouhadoun, A., Bassiouni, W., Goepf, M., Mani, S., Manikpurage, H.D., et al. (2020). International union of basic and clinical pharmacology. CIX. Differences and similarities between human and rodent prostaglandin E2 receptors (EP1–4) and prostacyclin receptor (IP): specific roles in pathophysiologic conditions. *Pharmacol. Rev.* **72**, 910–968.
- Qu, C., Mao, C., Xiao, P., Shen, Q., Zhong, Y.N., Yang, F., Shen, D.D., Tao, X., Zhang, H., Yan, X., et al. (2021). Ligand recognition, unconventional activation, and G protein coupling of the prostaglandin E2 receptor EP2 subtype. *Sci. Adv.* **7**, eabf1268.
- Ramlal, K., Palmer, C.M., Nakane, T., and Aylett, C.H.S. (2020). Mitigating local over-fitting during single particle reconstruction with SIDESPLITTER. *J. Struct. Biol.* **211**, 107545.
- Schorb, M., Haberbosch, I., Hagen, W.J.H., Schwab, Y., and Mastronarde, D.N. (2019). Software tools for automated transmission electron microscopy. *Nat. Methods* **16**, 471–477.
- Stallaert, W., Van Der Westhuizen, E.T., Schönege, A.M., Plouffe, B., Hogue, M., Lukashova, V., Inoue, A., Ishida, S., Aoki, J., Le Gouill, C., and Bouvier, M. (2017). Purinergic receptor transactivation by the β 2-adrenergic receptor increases intracellular Ca2+ in nonexcitable cells. *Mol. Pharmacol.* **91**, 533–544.
- Sugimoto, Y., Nakato, T., Kita, A., Takahashi, Y., Hatae, N., Tabata, H., Tanaka, S., and Ichikawa, A. (2004). A cluster of aromatic amino acids in the i2 loop plays a key role for gs coupling in prostaglandin EP2 and EP3 receptors. *J. Biol. Chem.* **279**, 11016–11026.
- Suto, F., Rowe-Rendleman, C.L., Ouchi, T., Jamil, A., Wood, A., and Ward, C.L. (2015). A novel dual agonist of EP3 and FP receptors for OAG and OHT: safety, pharmacokinetics, and pharmacodynamics of ONO-9054 in healthy volunteers. *Invest. Ophthalmol. Vis. Sci.* **56**, 7963–7970.
- Vecchio, E.A., Baltos, J.A., Nguyen, A.T.N., Christopoulos, A., White, P.J., and May, L.T. (2018). New paradigms in adenosine receptor pharmacology: allostery, oligomerization and biased agonism. *Br. J. Pharmacol.* **175**, 4036–4046.
- Weis, W.I., and Kobilka, B.K. (2018). The molecular basis of G protein-coupled receptor activation. *Annu. Rev. Biochem.* **87**, 897–919.
- Wise, A., Foord, S.M., Fraser, N.J., Barnes, A.A., Elshourbagy, N., Eilert, M., Ignar, D.M., Murdock, P.R., Steplewski, K., Green, A., et al. (2003). Molecular identification of high and low affinity receptors for nicotinic acid. *J. Biol. Chem.* **278**, 9869–9874.
- Xiao, P., Yan, W., Gou, L., Zhong, Y.N., Kong, L., Wu, C., Wen, X., Yuan, Y., Cao, S., Qu, C., et al. (2021). Ligand recognition and allosteric regulation of DRD1-Gs signaling complexes. *Cell* **184**, 943–956.e18.
- Xing, C., Zhuang, Y., Xu, T.H., Feng, Z., Zhou, X.E., Chen, M., Wang, L., Meng, X., Xue, Y., Wang, J., et al. (2020). Cryo-EM structure of the human cannabinoid receptor CB2-gi signaling complex. *Cell* **180**, 645–654.e13.
- Xu, P., Huang, S., Mao, C., Krumm, B.E., Zhou, X.E., Tan, Y., Huang, X.P., Liu, Y., Shen, D.D., Jiang, Y., et al. (2021). Structures of the human dopamine D3 receptor-Gi complexes. *Mol. Cell* **81**, 1147–1159.e4.
- Yin, J., Chen, K.Y.M., Clark, M.J., Hijazi, M., Kumari, P., Bai, X.C., Sunahara, R.K., Barth, P., and Rosenbaum, D.M. (2020). Structure of a D2 dopamine receptor–G-protein complex in a lipid membrane. *Nature* **584**, 125–129.
- Yuan, D., Liu, Z., Kaendli, J., Maeda, S., Zhao, J., Sun, X., Xu, J., Gmeiner, P., Wang, H.W., and Kobilka, B.K. (2020). Activation of the α 2B adrenoceptor by the sedative sympatholytic dexmedetomidine. *Nat. Chem. Biol.* **16**, 507–512.
- Zhang, K. (2016). Gctf: real-time CTF determination and correction. *J. Struct. Biol.* **193**, 1–12.
- Zheng, S.Q., Palovcak, E., Armache, J.P., Verba, K.A., Cheng, Y., and Agard, D.A. (2017). MotionCorr2: anisotropic correction of beam-induced motion for improved cryo-electron microscopy. *Nat. Methods* **14**, 331–332.
- Zhuang, Y., Xu, P., Mao, C., Wang, L., Krumm, B., Zhou, X.E., Huang, S., Liu, H., Cheng, X., Huang, X.P., et al. (2021). Structural insights into the human D1 and D2 dopamine receptor signaling complexes. *Cell* **184**, 931–942.e18.
- Zivanov, J., Nakane, T., and Scheres, S.H.W. (2019). A Bayesian approach to beam-induced motion correction in cryo-EM single-particle analysis. *IUCr* **6**, 5–17.
- Zivanov, J., Nakane, T., Forsberg, B.O., Kimanius, D., Hagen, W.J., Lindahl, E., and Scheres, S.H. (2018). New tools for automated high-resolution cryo-EM structure determination in RELION-3. *Elife* **7**, e42166–22.

STAR★METHODS

KEY RESOURCES TABLE

REAGENT or RESOURCE	SOURCE	IDENTIFIER
Chemicals, peptides, and recombinant proteins		
FLAG peptide	Scrum	N/A
EDTA-free complete inhibitor cocktail tablets	Roche	Cat# 05056489001
PGE ₂	Cayman	Cat#14010
DDM (n-Dodecyl-β-D-Maltopyranoside), Sol-Grade	Anatrace	Cat#D310S
LMNG (Lauryl Maltose Neopentyl Glycol)	Anatrace	Cat#NG310
GDN	Anatrace	Cat#GDN101
Sodium Cholate	Dojindo	Cat#C321
cholesterol hemi-succinate	Sigma	Cat#C6512
Cholesterol	Sigma	Cat#C8667
Iodoacetamide	Wako	Cat#093-02892
Ni-NTA Superflow	Qiagen	Cat#30450
Anti-FLAG M1 agarose affinity Gel	Sigma	Cat#4596
Sf9 expression medium	WAKO	Cat#160-25851
DMEM	Nacalai tesque	Cat#08456-65
PEI MAX	Polyscience	Cat#24765
D-luciferin	Wako	Cat#126-05116
PF-04418948	Cayman	Cat#15016
Forskolin	Wako	Cat#067-02191
Deposited data		
EP3-Gi signaling complex	This paper	PDB ID: 7WU9 EMD-32824 EMPIAR-11119
Software and algorithms		
SerialEM	Schorb et al. (2019)	https://bio3d.colorado.edu/SerialEM
Chimera		N/A
phenix.real_space_refine	Adams et al. (2010)	https://www.phenix-online.org/
Coot	Emsley et al. (2010)	https://www2.mrc-lmb.cam.ac.uk/personal/pemsley/coot/
RELION-3.1	Zivanov et al. (2018)	https://www3.mrc-lmb.cam.ac.uk/relion
Gctf	Zhang (2016)	https://www2.mrc-lmb.cam.ac.uk/research/locally-developed-software/zhang-software/#gctf
MotionCor2	Zheng et al. (2017)	https://emcore.ucsf.edu/ucsf-software
SIDESPLITTER	Ramlal et al. (2020)	https://github.com/StructuralBiology-ICLMedicine/SIDESPLITTER

RESOURCE AVAILABILITY

Lead contact

Further information and requests for resources and reagents should be directed to and will be fulfilled by the lead contact, Ryoji Suno (sunory@hirakata.kmu.ac.jp) and Takuya Kobayashi (kobayatk@hirakata.kmu.ac.jp).

Materials availability

This study did not generate new unique reagents.

Data and code availability

- The cryo-EM data generated in this study have been deposited into the Electron Microscopy Data Bank and Electron Microscopy Data Bank and Electron Microscopy Public Image Archive with accession numbers EMD-32824 and EMPIAR-11119.

- The 3D models reported in this paper have been deposited in the Protein Data Bank with accession code PDB ID: 7WU9.
- This paper does not report original code.
 - Any additional information required to reanalyze the data reported in this paper is available from the [lead contact](#) upon request.

EXPERIMENTAL MODEL AND SUBJECT DETAILS

Escherichia coli (*E. coli*) BL21-CodonPlus (DE3)-RIPL cells (Agilent Technologies) were cultivated in terrific broth (TB) supplemented with 100 mg/L ampicillin at 37°C. *Brevibacillus choshinensis* HPD31-SP3 competent cells were cultivated in 2SY medium supplemented with 50 mg/L neomycin at 30°C. *Spodoptera frugiperda* 9 (Sf9) insect cells were cultured in PSFM-J1 medium (Wako) supplemented with 2% fetal bovine serum (FBS) (Sigma), 50 units/mL penicillin, 50 µg/mL streptomycin (Wako), and 0.5 µg/mL amphotericin B at 27°C. Parental human embryonic kidney 293 (HEK293) cells and ΔG_s - HEK293 cells, devoid of G_{α_s} and $G_{\alpha_{off}}$ (Stallaert et al., 2017), were grown in Dulbecco's modified Eagle's medium (DMEM; Nacalai tesque) supplemented with 10% FBS (Nichirei Biosciences), 100 units/mL penicillin, and 100 µg/mL streptomycin (Nacalai tesque) at 37°C in a 5% CO₂ incubator.

METHOD DETAILS

Expression and purification

For the human EP3 construct, we replaced the region of b562RIL in the construct used in the previously reported crystal structure (PDB ID: 6AK3) with the wild-type sequence of EP3. The construct was expressed in Sf9 insect cells using the Bac-to-Bac baculovirus system (Thermo Fisher Scientific). Cells were infected at a density of $3-4 \times 10^6$ cells per mL and were grown for 70 h at 27°C. Cells were collected by centrifugation and stored at –80°C until use. The purification method of EP3-GFP was the same as previously reported EP3-bRIL (Morimoto et al., 2019).

The plasmid expressing G_{i1} was introduced into *E. coli* BL21-CodonPlus (DE3)-RIPL (Agilent Technologies). The cells were cultivated in TB supplemented with 100 mg/L ampicillin at 30°C. After the optical density of the broth at 600 nm wavelength reached at 0.8, 500 µM isopropyl β -D-1-thiogalactopyranoside (IPTG) was added and incubated overnight at 25°C. The cells were collected by centrifugation and stored at –80°C until use. The cells were suspended in buffer A (40 mM HEPES-NaOH (pH 7.5), 100 mM NaCl, 10 mM imidazole, 5 mM MgCl₂, 50 µM GDP, 25 U/L DNase I, and protease inhibitor cocktail, 100 µM DTT) and were lysed by sonication. The insoluble components were removed by centrifugation at 38,000 $\times g$ for 30 min at 4°C, and the supernatant was loaded onto a 5 mL Ni-NTA Superflow resin column (Qiagen). The resin was washed with 20 column volumes of buffer B (20 mM HEPES (pH 7.5), 100 mM NaCl, 40 mM imidazole, 1 mM MgCl₂, and 50 µM GDP), and the resin-binding protein was eluted in buffer C (20 mM HEPES-NaOH (pH 7.5), 100 mM NaCl, 500 mM imidazole, 1 mM MgCl₂, and 50 µM GDP). TEV protease was added to the eluate, and the eluate was dialyzed overnight against 2 L buffer D (20 mM HEPES (pH 7.5), 100 mM NaCl, 1 mM MgCl₂, 10 µM GDP) at 4°C. The sample was incubated with 5 mL Ni-NTA superflow resin to remove the contaminants bound to the resin, and the purified sample was collected as flow-through. The sample was concentrated and was further purified using a HiLoad 16/600 Superdex 200 pg (Cytiva) with buffer E (10 mM HEPES-NaOH (pH 7.5), 100 mM NaCl, 1 mM MgCl₂, 1 µM GDP, and 0.1 mM Tris [2-carboxyethyl] phosphine hydrochloride (TCEP)).

$G\beta_1\gamma_2$ heterodimer was expressed in Sf9 insect cells using the BestBac baculovirus system (Thermo Fisher Scientific). Sf9 insect cells were cultured in PSFM-J1 medium supplemented with 2% FBS, 50 units/mL penicillin, 50 µg/mL streptomycin, and 0.5 µg/mL amphotericin B. Sf9 cells at a density of $3-4 \times 10^6$ cells per mL were infected by viral stock at an MOI (multiplicity of infection) of 1. Infected cells were cultured at 27°C for 48–70 h. The cells were collected by centrifugation at 7,000 $\times g$ for 10 min and stored at –80°C until use. The cells were lysed in buffer F (10 mM Tris-HCl (pH 7.4), 0.1 mM MgCl₂, 10 mM 2-mercaptoethanol, 10 µM GDP, 1 mM benzamidin, and 2.5 µM leupeptin), and was homogenized with a Dounce homogenizer and centrifuged at 140,000 $\times g$ for 30 min at 4°C. The precipitate was suspended in buffer G (10 mM HEPES-NaOH (pH 7.5), 1 M NaCl, 20 mM KCl, 10 mM MgCl₂, 10 mM 2-mercaptoethanol, 10 µM GDP, 1 mM benzamidin, and 2.5 µM leupeptin), and centrifuged at 140,000 $\times g$ for 15 min at 4°C. The precipitate was solubilized in buffer H (20 mM HEPES-NaOH (pH 7.5), 100 mM NaCl, 5 mM MgCl₂, 0.05% DDM, 1% sodium cholate, 10 mM 2-mercaptoethanol, 10 µM GDP, 1 mM benzamidin, and 2.5 µM leupeptin) at 4°C for 1 h. The insoluble components were removed by centrifugation at 140,000 $\times g$ for 30 min at 4°C. Imidazole (final concentration of 20 mM) and Ni-NTA resin were added to the supernatant and incubated for 1 h at 4°C. Bound protein was first washed in a buffer H including 20 mM imidazole (final concentration), followed by washes in gradually decreasing sodium cholate concentrations, and then washed with buffer I (20 mM HEPES-NaOH (pH 7.5), 100 mM NaCl, 20 mM imidazole, 1 mM MgCl₂, 0.05% DDM, 5 mM 2-mercaptoethanol, 10 µM GDP). The resin was suspended in buffer I supplemented with 3C protease and then stirred gently overnight at 4°C. The flow-through was collected, the resin was washed with buffer I, and the flow-through was collected. The collected sample was concentrated to about 1 mg mL^{–1} using a centrifugal filter device (50 kDa MW cutoff, Millipore).

The scFv16 was produced by secretion from the Gram-positive bacterium *Brevibacillus choshinensis*. The gene encoding scFv16 was synthesized and inserted downstream of and in frame with the secretion signal sequence of the plasmid pNY326 (Takara-Bio/Clontech). To facilitate the detection and purification of the secreted proteins, sequences for the TEV protease cleavage site and a mCherry-His₆ tag were placed at the C-termini of the scFv16 cDNAs. *B. choshinensis* cells harboring the scFv16-expression plasmid

were grown at 30°C with shaking at 200 rpm in 2SY medium (soytone 40 g/L, yeast extract 5 g/L, glucose 20 g/L, and CaCl₂ 0.15 g/L) supplemented with 50 mg/L neomycin for 65–70 h. The recovered culture supernatant was adjusted to a final ammonium sulfate concentration of 60% saturation. The precipitate was pelleted, dissolved in TBS buffer (10 mM Tris-HCl, pH 7.5, 150 mM NaCl), and dialyzed overnight against the same buffer. The dialyzed sample was purified with Ni-NTA resin, mixed with TEV-His₆ and dialyzed overnight again against TBS buffer. The cleaved mCherry-His₆ tag and TEV-His₆ were removed using a HisTrap column. The flow-through fractions were further purified with a HiLoad 16/600 Superdex 75 pg column (Cytiva) equilibrated with TBS buffer. The peak fractions were pooled, concentrated, flash frozen in liquid nitrogen, and stored at –80°C.

Formation and purification of the human EP3-G_{i1}Gβ₁γ₂-scFv16 complex

Purified G_{i1} and Gβγ were mixed at the molar ratio of 1:1.2 to form G_{i1} heterotrimer, and the mixture was purified by size-exclusion chromatography on Superdex 200 increase 10/300 GL (Cytiva) using a buffer containing 20 mM HEPES-NaOH (pH 7.5), 100 mM NaCl, 1 mM MgCl₂, 10 μM GDP, 0.1 mM TCEP, 0.02% DDM, and 0.004% Cholesteryl hemisuccinate (CHS) (Merck). Peak fractions of G_{i1} heterotrimer were pooled and concentrated to 1 mg mL^{–1} using a centrifugal filter device (50 kDa MW cutoff, Millipore). The purified EP3-GFP was mixed with a 1.2 molar excess of G_{i1} heterotrimer, and the complexing mixture was incubated in the presence of 1 μM PGE₂ for 3 h at room temperature. Apyrase (New England Biolabs) was added to catalyze hydrolysis of unbound GDP. After 1 h of incubation at 4°C, the mixture was loaded onto NHS-activated Sepharose resin (Cytiva) coupled with a GFP-binding nanobody provided by Dr. Hino (Tottori University). The resin was washed with buffer containing 20 mM HEPES-NaOH (pH 7.5), 100 mM NaCl, 0.01% 2,2-didecylpropane-1,3-bis-β-D-maltopyranoside (LMNG), 0.0033% GDN, 0.002% CHS, and 10 μM PGE₂ for ten column volumes. The washed resin was treated with 3C protease and incubated at 4°C overnight. The elution was mixed with a two-molar excess of scFv16 and the mixture was incubated for 1 h at 4°C. The mixture was then concentrated and purified by size-exclusion chromatography using Superdex 200 increase 10/300 GL (Cytiva) using a buffer containing 20 mM HEPES-NaOH (pH 7.5), 100 mM NaCl, 0.00075% LMNG, 0.00025% GDN, 0.0001% CHS, and 10 μM PGE₂. Peak fractions were pooled and concentrated to 10 mg mL^{–1} using a centrifugal filter device (100 kDa MW cutoff, Millipore).

Cryo-EM grid preparation and data collection

Two μL of the sample solution was applied to a glow-discharged QUANTIFOIL R1.2/1.3 Cu 300 mesh grid (Quantifoil Micro Tools GmbH, Germany). After blotting the excess solution on the grid with filter paper, the samples were rapidly frozen in liquid ethane using a Vitrobot Mark IV (Thermo Fisher Scientific). The frozen grids were screened to check sample conditions such as the ice thickness and particle dispersity using a Talos Arctica cryo-transmission electron microscope (cryo-TEM) operating at 200 keV and equipped with a Falcon 3 direct electron detector (Thermo Fisher Scientific) at Institute for Protein Research, Osaka University. Cryo-EM data collection was performed on a Titan Krios cryo-TEM equipped with a Cs corrector (Thermo Fisher Scientific) operating at 300 keV in EFTEM nanoprobe mode at Institute for Protein Research, Osaka University. Images were acquired as movies using Gatan BioQuantum energy filter (slit width of 20 eV) and K3 direct detection camera (Gatan, Inc., USA) in electron counting mode. A total of 10,241 movies were collected at a dose rate of 12.9 e[–]/pixel/s, a pixel size of 0.675 Å², and a total dose of 75 e[–]/Å². SerialEM software (Schorb et al., 2019) was used for automated data collection using a 3x3-hole pattern beam-image shift scheme with a nominal defocus range of –0.7 to –1.5 μm.

Image processing

Image processing was performed with RELION-3.1 (Zivanov et al., 2018). With the wrappers in RELION, movie frames were gain-normalized, aligned, dose-weighted, and summed using MotionCor2 (Zheng et al., 2017), and defocus values were estimated using Gctf (Zhang, 2016). Automatic particle picking was performed with the RELION's Laplacian-of-Gaussian (LoG) approach to obtain 2D class averages for reference. Using these 2D class averages as template, reference-based automatic particle picking was performed, and 2,028,191 image segments were extracted. The extracted images were submitted to several rounds of 2D and 3D classifications to remove junk images. The selected 1,090,904 particles were then subjected to 3D auto-refinement yielding a 3D reconstruction at 4.5 Å resolution. The 795,617 particles were further classified by a masked 3D classification without alignment. After a Bayesian polishing step (Zivanov et al., 2019), 3D auto-refinement with the reconstruction algorithm SIDESPLITTER (Ramlaul et al., 2020) was performed with 125,572 particles, and yielded a 3D reconstruction at 3.4 Å resolution. The algorithm relion_postprocess was used to calculate the local resolution, and to provide a locally-sharpened map using a B-factor of –113 Å², which was used as the final map. The image processing steps are summarized in Figure S2.

Model building and refinement

The atomic model building was performed by manual iterative building in Coot (Emsley et al., 2010), followed by refinement with phenix.real_space_refine in the Phenix program suite (Adams et al., 2010). In this model, 97% of the residues were in favored regions of Ramachandran plot, and all the others were in allowed regions. Refinement statistics are shown in Table S3.

Signaling assay

To evaluate GPCR-mediated cAMP signaling, we use Promega's split luciferase-based GloSensor cAMP biosensor technology. HEK293 cells were seeded into the 6-well plates at a density of 5 × 10⁵ cells/well. For G_s activity estimation which was performed

24 h post-seeding, 500 ng of EP3 or 50 ng of EP4 plasmid was co-transfected with 1.5 μ g of pGloSensorTM-22F cAMP plasmid (Promega) into parental HEK293 cells using polyethylenimine (PEI MAX; Polyscience). After 24 h post transfection, transfected cells were washed once with PBS and detached using 0.53 mM EDTA. Cells were harvested with centrifugation at $200 \times g$ for 5 min and resuspended in Hank's balanced salt solution (HBSS; Thermo Fisher Scientific) containing 5 mM HEPES (pH 7.4). Approximately 50,000 to 100,000 cells per well were distributed in 96-well flat-bottomed white microplates (Greiner Bio-One) and treated with 1 mM D-luciferin (FUJIFILM Wako Pure Chemical) and 10 μ M PF-04418948 (EP2 antagonist for inhibition of endogenous EP2 activities; Cayman Chemical). Following incubation for 2 h at room temperature, luminescence was monitored continuously on a Spectramax L (Molecular Devices) at room temperature. Ten μ L of PGE₂ was applied to cells in 100 μ L solution per well. For G_i activity measurement, 50 ng of EP3 plasmid was co-transfected with 1.5 μ g of pGloSensorTM-22F cAMP, G_s Δ Ct, and Ric8B plasmids into Δ G_s-HEK293 cells. Δ G_s-HEK293 cells were used to eliminate the activation of G_s by EP3. G_s Δ Ct, which lack 7 amino acids at the C-terminus and is thus unable to bind to GPCRs, was used as allosteric activator for adenylyl cyclase, while G_s Δ Ct is not activated by GPCRs due to the lack of C-terminus. Ric8B was used as a chaperone protein for G_s Δ Ct. After an incubation period of 2 h with D-luciferin, transfected cells were treated with PGE₂ and 10 μ M Forskolin (adenylyl cyclase activator). The inhibition of luminescence elevation was evaluated as G_i activity.

QUANTIFICATION AND STATISTICAL ANALYSIS

In signaling assay, maximum luminescence intensity post stimulation was quantified. The luminescence intensity reached a plateau about 10 min after stimulation. Each point represents the mean value \pm s.e.m. All the measurements were performed in triplicate. Sig-moid curve fitting was performed with Prism 7 (GraphPad).